Fluid Transport and Storage in the Cascadia Forearc inferred from Magnetotelluric Data

Gary Egbert
Oregon State University
Bo Yang (0016220@zju.edu.cn)
Zhejiang University https://orcid.org/0000-0001-6790-9882
Paul A. Bedrosian
USGS Denver https://orcid.org/0000-0002-6786-1038
Kerry Key
Columbia University https://orcid.org/0000-0003-1169-6683
Dean Livelybrooks
University of Oregon
Adam Schultz
Oregon State University
Anna Kelbert
United States Geological Survey
Blake Parris
University of Oregon

Article

Keywords: geodynamics, tectonics, subduction

Posted Date: June 22nd, 2021

DOI: https://doi.org/10.21203/rs.3.rs-475649/v1

Version of Record: A version of this preprint was published at Nature Geoscience on July 14th, 2022. See the published version at https://doi.org/10.1038/s41561-022-00981-8.

Fluid Transport and Storage in the Cascadia Forearc inferred from Magnetotelluric Data

G. Egbert[1] ,B. Yang*[2], P. Bedrosian[3], K. Key[4],
D. Livelybrooks[5], A. Schultz[1,7], A. Kelbert[6], B. Parris[5]
[1] Oregon State University, Corvallis OR, USA,
[2] Key Laboratory of Geoscience Big Data and Deep Resource of Zhejiang Province, School of Earth Sciences, Zhejiang University, Hangzhou, China,
[3] USGS, Denver CO, USA
[4] Lamont-Doherty Earth Observatory, Columbia University, Palisades NY, USA
[5] University of Oregon, Eugene OR, USU
[6] USGS, Golden CO, USA
[7] Pacific Northwest National Laboratory, Richland, WA, USA

June 17, 2021

Abstract

Subduction of hydrated oceanic lithosphere can carry water deep into the Earth, with important consequences for a range of tectonic and magmatic processes. Most fluid is released at relatively shallow depths in the forearc where it is thought to play a critical role in controlling mechanical properties and seismic behavior of the subduction megathrust. Here we present results from three-dimensional inversion of nearly 400 long-period magnetotelluric sites, including 64 offshore, to provide new insights into the distribution of fluids in the forearc of the Cascadia subduction zone. Our amphibious dataset provides new constraints on the geometry of the electrically resistive Siletzia terrane, a thickened section of oceanic crust accreted to North America in the Eocene, and the conductive accretionary complex, which is being underthrust all along the margin. Fluids accumulate, over time-scales likely exceeding 1 My, above the plate interface in metasedimentary units, while the mafic rocks of Siletzia remain dry. Fluids in metasediments tend to peak at fixed slab-depths of 17.5 and 30 km, suggesting control by metamorphic processes, but also concentrate around the edges of Siletzia, suggesting that this mafic block is impermeable, with dehydration fluids escaping up-dip along the megathrust. Our results demonstrate that lithology of the overriding crust can play a critical role in controlling fluid transport and sequestration in a subduction zone, with potentially important implications for mechanical properties.

1 Introduction

Cascadia is an end-member subduction zone with a very young and hot subducting plate, capable of producing very large (Mw 9) megathrust earthquakes [1]. The central forearc crust, generically referred to as Siletzia [2], is a thickened section of oceanic crust that accreted to North America in the late Eocene (Fig. 1). The late-Tertiary Klamath [3], and Wrangellia [4] terranes, respectively form the southern and northern domains of the Cascadia forearc. Seismic refraction profiles [5] suggest that Siletzia is thickest in central-northern Oregon and thins to the north. In the Olympic peninsula the full crustal section is formed from accreted Tertiary sediments and metasediments, backstopped in the east by a thick section of Siletzia, which has been heavily deformed and tilted past vertical [6].

Cascadia is an archetype for episodic tremor and slip (ETS), characterized by bursts of non-volcanic seismic tremor accompanied by low-frequency earthquakes and geodetically detected slow slip [7] at or above the plate interface. There is substantial evidence [8–10] that ETS occurs where effective stresses are orders of magnitude less than lithostatic, which is most readily explained by overpressured fluids along or near the megathrust. Indeed, a low velocity layer (LVL) with anomalously high Poisson's ratios, also attributable to overpressured fluids [11], has been detected within, or slightly above, the subducting oceanic crust in Cascadia [12–14].

Although ETS occurs essentially everywhere in Cascadia, there are significant along-margin variations, with reduced intensity and longer recurrence intervals beneath the thickened central core of Siletzia in north-central Oregon [15]. The same area is almost devoid of crustal and intraplate seismicity [16], and may be more weakly coupled in the seismogenic locked zone [17]. This correlation of forearc crustal geology with patterns of ETS, seismicity, and plate locking has often been ascribed to variations in fluid pressure along the megathrust, due either to lithologically-controlled variations in crustal permeability [15, 17, 18], or variable hydration of the incoming plate [19–23].

Seismic imaging provides numerous indirect constraints on fluids and fluid-mediated processes in subduction zones, allowing estimates of the abundance of hydrous minerals in the subducting

plate [20, 24], forearc crust [25, 26], and forearc mantle [27], fluid content and consolidation in the accretionary prism [22, 28], and volumes of over-pressured fluids near the megathrust [11, 12, 29, 30]. Magnetotelluric (MT) imaging of electrical resistivity can provide more direct constraints on the present distribution and connectivity of free fluids in the crust. Previous MT studies in Cascadia have suggested along-margin variations in sediment subduction, high concentrations of fluids near the ETS zone, and evidence for flux melting beneath the arc [31–35]. Here we present new detailed images of electrical resistivity in Cascadia, based on three-dimensional (3D) inversion of 393 long-period MT sites (Fig. 1). The dataset includes 64 new offshore sites, extending from the trench to the coast, 102 new onshore sites, as well as all available long-period MT sites from legacy land profiles throughout the region [32], and 144 sites from the EarthScope MT transportable array [36]. Although the modeling domain extends from spreading ridge to back arc, and from northern California to southern British Columbia, our focus here is on the forearc in Oregon and SW Washington, where data density is highest. Details on the dataset and the inversion approach are provided in Methods and the supplemental material (SM).

2 Results

Our preferred 3D inverse solution is shown in Fig. 2, with a more complete set of model sections provided in Fig.

Fig. 2 reveals a conductive body (C1), extending from offshore to an abrupt landward termination beneath a massive resistive body (R1). We interpret C1 to represent fluid-rich sedimentary and metasedimentary rocks of the accretionary complex, and R1 to represent comparatively dry mafic rocks of Siletzia. Indeed, the geometry of R1 is broadly consistent with geological and geophysical constraints on Siletzia, including spatial extent [37], greater thickness in Oregon [5], and significant disruption and unroofing of the mafic section in the Olympic peninsula [6, 38] (R2). In Oregon and southern Washington Siletzia is very thick in the east, thinning abruptly to $\sim$10 km in a layer that extends offshore. The conductive accretionary complex is thrust a significant distance ($\sim$50 km, more in places) under this thin layer, terminating at the nearly vertical edge of R1. Offshore, conductivity of C1 is highest from 44-47°N; however, this may reflect limited offshore data coverage outside of this area (Fig. 1). A deeper, higher amplitude, peak in conductivity

(C2) occurs in all sections shown at a slab interface depth of 30-35 km, sometimes shallower. C2 commonly appears as a second peak within a broader conductive layer encompassing C1. Finally, there are conductive upwellings (C3) that rise towards the surface beneath the Cascade arc, beyond the eastern edge of Fig. 2. These arc conductive features [32] can be seen more clearly in Fig.

Resistive material extends beyond the southern edge of Siletzia into the Klamath terranes but changes to a relatively thin upper crustal layer (R3). Resistivity variations in this area are complex (Fig.

To provide a more complete view of the geometry of key features, we derive two plan-view images from the 3D resistivity model. First, we compute the depth extent of the resistors (R1-R4), defined by the bottom of the 300 ohm-m isosurface. Fig. 3a shows that Siletzia is 30-40 km thick within a series of discrete blocks (a-e), distributed from Puget Sound to its southern edge, where a resistive curtain extends to the plate interface (f). This 3D image substantially revises previous models of Siletzia as a relatively uniform thick mafic block that thins to the north [5]. It is consistent with tomographic images [26] which show patches of high Vs just above the plate interface, coincident with thickened blocks of Siletzia. There is a sharp transition from the thin outboard edge of Siletzia to the much thicker blocks to the east, marking the abrupt termination of the underthrust accretionary complex. One exception to this picture occurs in central Oregon, where a resistive body near the coast (g) extends to the plate interface, with thinner Siletzia to the east underlain by a shallow conductor (R4/C2 in Fig. 2).

The geometry of Siletzia revealed here is consistent with its hypothesized origin as a chain of seamounts [39] or an oceanic plateau [40]. Plausibly, the deep resistive patches represent the roots of individual eruptive centers. Subsequent middle-Eocene basaltic magmatism [2] may also have contributed to the deep geometry of the resistive body, for example feature g in Fig. 3a. There is a strong correlation between the imaged thickness of Siletzia and modern tectonic and magmatic activity. Faults in the forearc crust [18] often trace the edges of the thickest resistive blocks, and tend to concentrate where Siletzia is thin (Fig. 3a). Variations in the western limit of arc volcanism further correlate with the eastern edge of thick resistive material, with the most westerly eruptive vents always occurring where Siletzia is thin or absent, providing evidence for the role of pre-existing crustal structure in controlling modern magmatic processes [41].

A second view of the 3D model is provided by a 2D map of conductance integrated from the plate interface (Fig. 3b) to 10 km above it. A series of high-conductance features elongated parallel to slab contours, and aligned with the outer edge of Siletzia, extend from 45°-48°N (Fig. 3b, A-C). The northern terminus of this band coincides with the limit of densest data coverage and is not well constrained. To the south, the band continues (I), albeit with decreased conductance near 45°N. Downdip extents are variable, ranging from 35 km in the Olympic Peninsula, to 20 km in central Oregon. Except in the Olympic peninsula, these high conductance features are abruptly truncated by the thickened sections of resistive Siletzia (Fig. 3a), suggesting the downdip extent of subducted metasediments is primarily controlled by the deep geometry of Siletzia. In central Oregon structure is more complex: conductive feature D is somewhat deeper (35 km slab depth) and sits in the "cavity" formed by deep resistive features a, b, g. Along the southern edge of Siletzia a thin band of high conductance (E) is located just updip and north of the resistive curtain (f in Fig. 3a).

Conductance above the plate interface is systematically enhanced in three zones: offshore (G, H, I), near the forearc mantle corner (FMC; A, B, C, D, F), and beneath the arc. As illustrated in Fig. 4a, conductance typically peaks at three nominal slab depths: 17.5 km, 30 km, and 65 km. The central peak (nearest the FMC) is typically highest and exhibits significant variations in depth. Depths for the seaward peak are more constant, 15-20 km, with conductance always decreasing trenchward. The third peak, beneath the arc, is much broader and exhibits significant variations with latitude. Here we restrict our attention to the two forearc peaks, which are plotted on a map of ETS density in Fig. 3c. In the Klamath terrane almost all forearc conductance peaks occur at nominal depths of 17.5 and 30 km, at least north of 42°N where we have good data coverage. In contrast, the depths of conductance peaks are more variable beneath Siletzia. Between 45°N and the southern Siletz margin, the seaward edge of resistive block a extends up-dip to 40 km, and conductance peaks are centered at depths of 17.5 and 35 km, similar to beneath the Klamaths. However, where resistive blocks b, c and d extend further up-dip, the inboard peak is deflected seaward to slab depths as shallow as 20 km.

As in previous works [32] we interpret the imaged conductive features to reflect fluids released from the subducting plate through sediment compaction, dehydration of clay minerals, pore collapse in meta-basalts, and a series of prograde metamorphic reactions [28, 42, 43]. Although these processes overlap in P/T space, pulses of fluid release are expected, as mechanical thresholds and the stability fields for different mineral assemblages are crossed [44, 45]. The observed characteristic depths for enhanced conductivity likely reflect these facies transitions. However, along-margin variations in lithology will further control the transport and accumulation of fluids, and we argue that these variations play a key role in determining the spatial pattern of imaged conductive anomalies and hence the distribution of subduction-zone fluids.

3 Discussion

Conductivity in the forearc crust varies by over three orders of magnitude, often abruptly. We believe these differences are most reasonably explained by variations in lithology and their corresponding changes in fluid content, especially given substantial seismic and geodynamic evidence for fluids in the megathrust [12, 29, 30] and in the overriding crust [25, 26]. Assuming resistivity can be taken as an indicator of lithology, the MT images provide important new constraints on the structure, creation, and evolution of the forearc crust. Most obviously, our results support previous suggestions [46, 47] that the entire Cascadia margin is being underthrust by accretionary complex material, driving uplift of the Coast Ranges [47, 48]. The 3D geometry of resistive Siletzia, segmented into thick, fault-bounded blocks, also provides clues to the genesis and accretion of this terrane and is deserving of further study.

The pattern of conductive features near the plate interface places constraints on fluid pathways, storage, and egress. Fluid inputs at the trench include pore water and hydrous minerals, both in the sediment layer, and in the underlying mafic oceanic crust. Free water in sediments is lost through compaction at depths < 10 km [28, 49], and is thus not a likely source for the patches of high conductivity, which are all deeper. Similarly, dehydration of clay minerals should be largely complete at temperatures of $\sim$150°C, which in Cascadia is well above the depth of the imaged conductors.

That there is a peak in conductance at a relatively constant slab depth centered at $\sim$17.5 km suggests a possible fluid source at corresponding P/T conditions. We suggest this peak may at least in part result from pore collapse in the meta-basalts, which is believed to occur at temperatures of 200-400°C [28, 44]. Our results may thus provide an important constraint on this poorly understood process.

The highest peaks in above-slab conductance at 20-35 km depth almost certainly reflect fluids released from meta-basalt dehydration. The subducting oceanic crust is relatively dry in Cascadia, with at most 5 vol% structural water [20]. We show in the SM that the implied rate of fluid input, together with estimates of the fluid volume required to explain observed conductance (Fig. 4a), places a lower bound on fluid residence times of $\sim$1 My. Thus, the main conductive features in Fig. 3b represent areas where fluids are sequestered on long timescales but they are not necessarily coincident with source regions.

Within Siletzia the main areas of fluid storage are just up-dip of thickened resistive crust that extends vertically to near the plate interface. We suggest that the sequestered fluids are sourced by dehydration reactions occurring at a relatively constant range of slab depths, 35 km and below, near the FMC [50]. We further suggest that Siletzia is relatively impermeable. Where these rocks extend to near the plate interface fluids are transported up-dip along the megathrust, ultimately leaking out along the outer edge where they accumulate in adjacent metasediments. Further support for this conclusion is provided in Fig. 4b, where we plot above-slab conductance (Fig. 3b) averaged in non-overlapping strips centered upon the 22.5 and 32.5 km slab contours. An inverse correlation is evident; at latitudes where conductance is low along the deeper contour (i.e., where fluids do not accumulate in the overriding crust near the source), conductance (and by inference fluid accumulation) is increased up-dip. Even where the roots of Siletzia do not extend to the plate interface, as in the Puget Sound area, or are absent altogether (the Klamath terranes), peak conductance always occurs up-dip of the FMC (Fig. 3c), where tremor intensity is greatest and fluid pressures are presumably greatest. In fact, meta-basalt dehydration reactions occur over a range of depths, near and down-dip from the zone of maximum tremor [24, 43, 50]. Fluids escaping into the crust likely move more rapidly up-dip than vertically, due to strong permeability anisotropy

along and near the plate interface. In all cases fluid accumulation must reflect transport history as an integral over source depths and time. The resulting conductance peaks are thus shifted systematically up-dip, relative to the fluid source. This shift is most extreme, and highly variable, where resistive Siletzia extends landward into the region where dehydration fluids are generated.

Seismically imaged low-velocity layers (LVLs) near the plate interface in Cascadia [12, 14, 24, 25, 29, 51] and elsewhere [30, 52], have been interpreted either as a thin layer of fluid trapped in the upper oceanic crust [52], or a thicker zone of fluid-saturated metasediments in the overriding crust [25, 53, 54]. The MT results clearly support the latter view but are not necessarily inconsistent with the former. Fluid porosity in the LVL beneath Vancouver Island has been estimated to be 2.7-4% [29]. Assuming $\sigma_f = 30$ S/m and an Archie's law exponent $m = 1.5$, a 5-km thick layer would have a conductance of 400-800 S, which if present everywhere, as some have argued[13, 14], would be resolved by our data . A thinner (e.g., 1 km) less saline layer would have a conductance of $\sim$ 100 S, and could be present over much of the forearc without violating the MT data (Fig. 3b).

Seismic reflection images [53, 55] from northern Cascadia may provide insight into the nature of the conductive underthrust rocks. A zone of high reflectivity (the E-layer), interpreted as a zone of strongly sheared metasediments with sub-horizontal fluid-filled cracks, thickens from 2 km offshore where the megathrust is locked, to a thicker (5-7 km) layer inland where deformation becomes aseismic [53]. The conductive zones in Fig. 3b are likely similar, representing thick layered metasedimentary packages that are ductile, strongly sheared, laminated, and filled with fluids. Indeed, the E-layer beneath Vancouver Island is conductive [54, 56].

As others have noted [15, 18, 26], there is a significant reduction in ETS frequency between 43-47°N (Fig. 3c), coincident with the thickest parts of Siletzia (Fig. 3a). This has often been ascribed to reduced fluid pressures in this area, due either to reduced oceanic plate hydration [23] or permeability [16], or to enhanced fluid leakage into the overriding crust [18]. However, our results are consistent with a more uniform dehydration fluid source (e.g., note the relative uniformity of total fluid storage along margin implied by Fig. 4b), and a more impermeable forearc crust in Siletzia. Thus, fluid pressures near the FMC might be expected to be at least as high beneath

Siletzia as to the north or south. A source of fluid is a necessary, but not sufficient, condition for ETS, which most likely results from complex interactions in the stressed rock/fluid system [57], with cyclic fluctuations in fluid pressure driven by fracturing and fluid movement, followed by crack sealing by mineral precipitation [58, 59]. Our results suggest that variations in lithology, with corresponding variations in rheology, rock strength, and mineral dissolution and precipitation kinetics, may in fact be the primary driver of along-margin variations in ETS intensity in Cascadia. For example, there is some evidence that localized heterogeneity in the fault zone, with stronger asperities embedded in a more easily deformed matrix, may be a requirement for ETS [57, 60]. Thus, one possibility is that fault zone heterogeneity is reduced in north-central Oregon. Here Siletzia extends to near the plate interface, perhaps resulting in a narrower and more strongly sheared subduction channel, with fewer large asperities. It is also possible that transverse permeability of this more focused subduction channel is enhanced, allowing more rapid updip fluid escape, and reduced fluid pressures in the ETS zone.

To make further progress on understanding ETS in Cascadia the MT images should be more fully integrated with other geophysical constraints, especially more detailed seismic imaging and geodynamic models. In particular, the accretionary complex (mostly, but not completely, metasediments) and the competent rocks of Siletzia apparently have vastly different capacities for fluid storage, allowing MT to effectively map lithology. As these units will also differ greatly in their rheological properties, the resistivity maps could have important implications for geodynamic modeling of the subduction zone [61], and may ultimately provide an improved understanding of variations in seismicity and plate coupling along the margin.

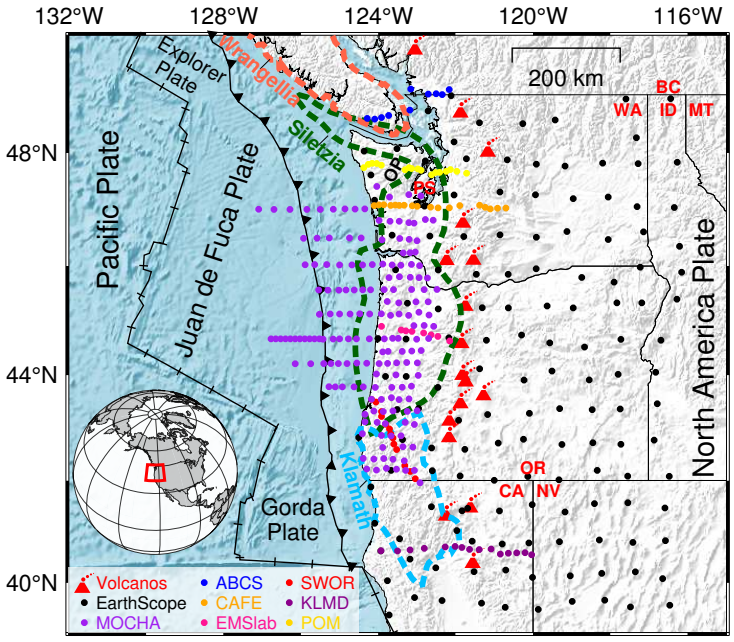

Figure 1: Map of study area, including tectonic plates, arc volcanoes (red triangles), state or provincial boundaries, and topography shown by shaded relief. Inset shows location on west coast of North America. Geologic terranes are outlined with dashed lines and labeled by color. Small filled circles show MT site locations, with different colors for each data source, as indicated in legend. Olympic Peninsula (OP) and Puget Sound (PS) are marked in the northern part of Siletzia.

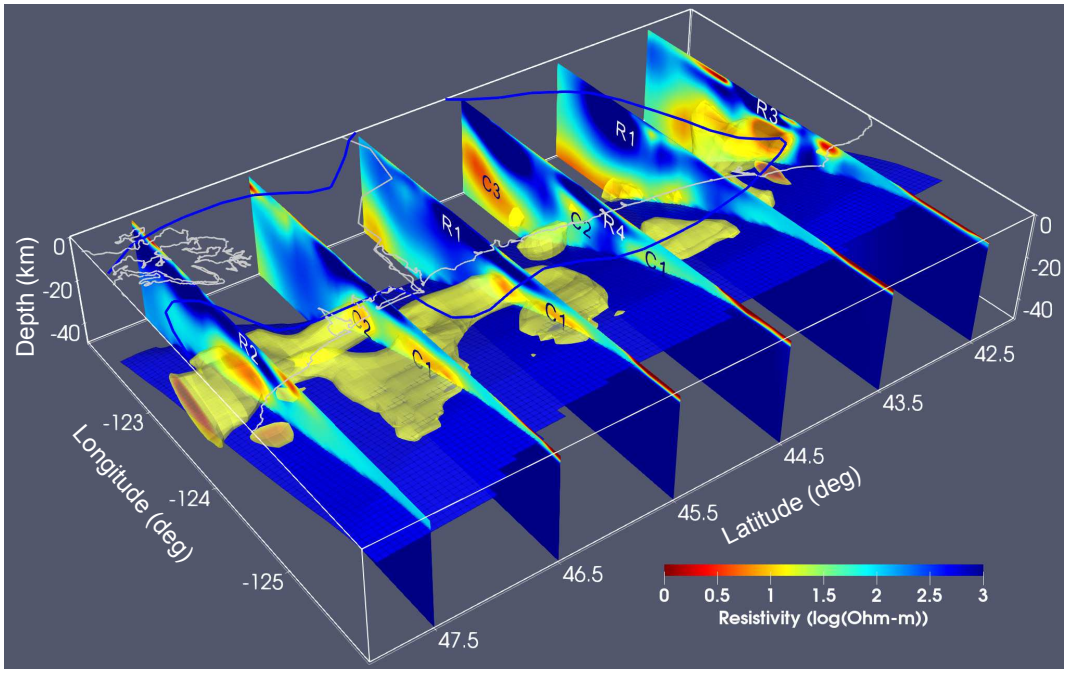

Figure 2: Three-dimensional view of the forearc portion of the model, including cross-sections at 1 degree increments, with superimposed iso-surface for conductive ($\rho < 16$ ohm-m) material. Curved blue hatchured surface marks the top of subducting plate, from the model of [62]. Coastlines and state borders are shown with white lines, and the outline of Siletzia, as defined in [37] by the heavy blue line, both at $z = 0$. Principal conductive and resistive features discussed in text are labelled C1-C3, and R1-R4, respectively.

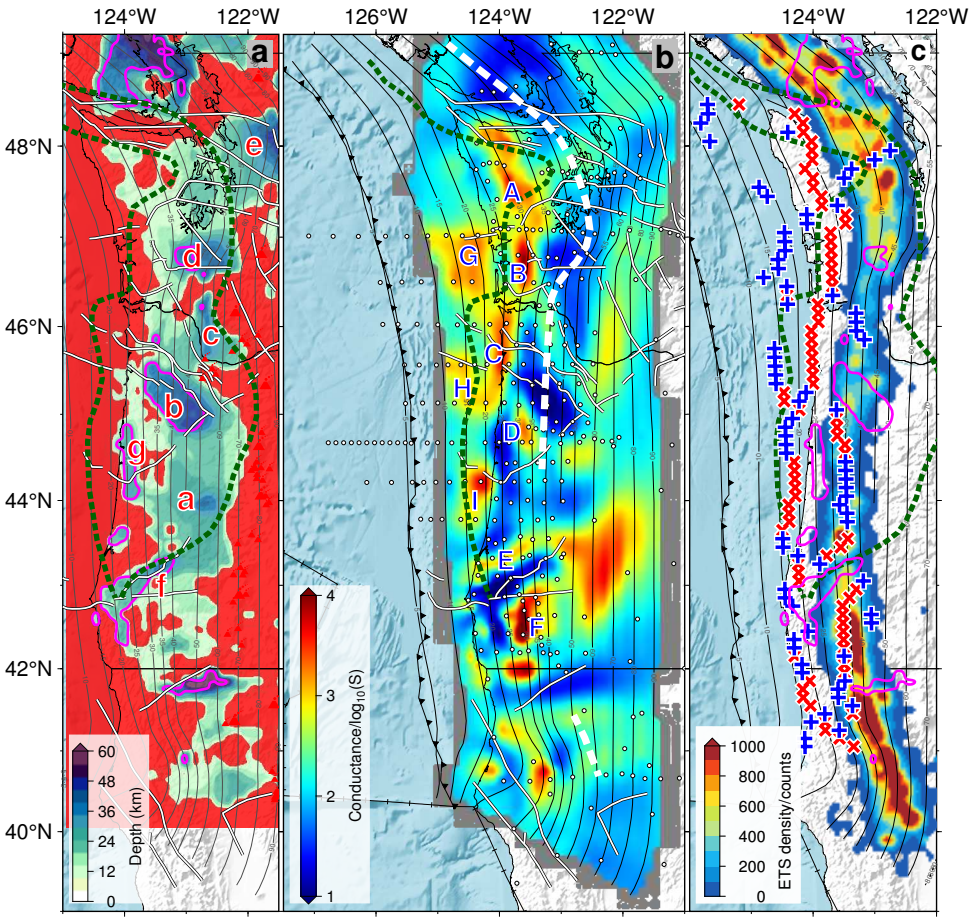

Figure 3: (a) Depth to bottom of the 300 ohm-m isosurface for the preferred model shown in Fig. 2. Examination of cross sections (see Fig.

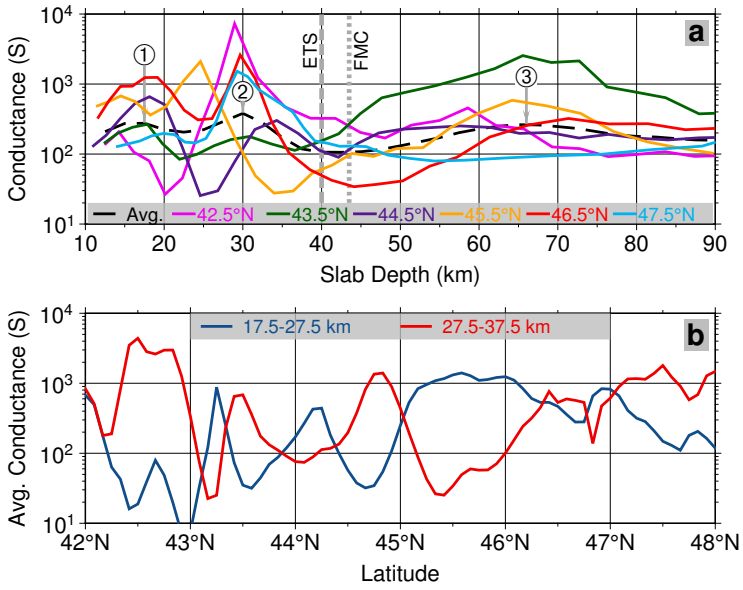

Figure 4: (a) Profiles of conductance as a function of slab depth at latitudes corresponding to sections shown in Fig. 2 (colored lines), and average computed along depth contours (black dashed line). The three nominal peaks (seaward, FMC, and arc) are marked as 1, 2, 3 respectively. Mean slab depth of peak ETS density and FMC position are also marked. (b) Conductance plotted in Fig. 3b, averaged over non-overlapping bands of slab depths (17.5-27.5 and 27.5-37.5 km).

4 Methods

MT data and inversion. Our MT dataset includes 165 new sites (including 64 offshore) from the "MOCHA" (Magnetotelluric Observations of Cascadia with a Huge Array) project, straddling the continental margin in the central part of the Cascadia subduction zone (Fig. 1). These were supplemented with 142 EarthScope transportable array MT sites [36], and legacy long-period data from six 2D profiles (13 from EMSLAB [31], 18 from CAFE-MT [35], 13 from SWORMT [63], 15 from KLMD [32], 17 from POM [64], and 10 from ABCS [33]). Most of the profile data are discussed in ref. [32]. For the MOCHA onshore sites and the five profiles, site spacing is typically 10-20 km, while for the offshore sites, profiles are 40 km apart, with 20 km site spacing, except for the central profile at 44.25°N with a denser site spacing of 5 km. In total there are 393 long-period MT sites, with data covering the period ranging from 7 s to 14,678 s. All onshore sites measured vertical magnetic fields; offshore sites did not. Data were processed with standard robust processing algorithms [65, 66].

For 3D inversion we use the ModEM code [67]. This inversion code allows specification of

a prior model, deviations from which are penalized by the regularization. For results reported here the prior model consists of a layered 1D earth with resistivity 100 ohm-m to a depth of 410 km, 10 ohm-m from there to 660 km, and 3 ohm-m below this. In the first layers of the starting model we included known bathymetry with the resistivity of seawater set to 0.3 ohm-m [68]. We also included a realistic ocean sediment distribution [69], with electrical resistivity of the saturated sediments set to 1 ohm-m.

Finally, we included the subducting Juan de Fuca plate in the prior model as a dipping resistive layer, as in [35]. There is substantial evidence that oceanic lithosphere is generally quite resistive [70]. While resistive bodies are observed in MT inversions over subducting plates [32, 71] without imposing this structure, MT data cannot vertically resolve resistive bodies. Imposing the seismically-constrained geometry of the plate in the prior model can improve resolution of conductive features above the plate. We take depth to the top of the shallower parts of the plate (above 90 km) from ref. [62], and extend to greater depths using seismic tomographic models [72]. Thickness of the plate was set to 50 km based on published models of resistive ocean lithosphere [73]. The assumed prior model is summarized graphically in Fig.

The model grid has a resolution of 11×9.5 km horizontally, with vertical layers logarithmically spaced, starting from very fine layers (20 meters) to discretize the bathymetry and the seafloor sediments. The resulting core grid is $120\times108\times57$ cells in latitude, longitude and depth respectively. Edges were padded with 7 logarithmically increasing grid cells on all sides, to extend the boundary of the study area $\sim$600 km in all directions. We ran the inversion more than 30 times, to test effects of various parameters (e.g., thickness of the slab, effect of offshore sites, effects of seafloor sediments, covariance parameters) and inversion strategies.

The seafloor data presented some challenges to the 3D inversion. Lack of short period data makes it difficult to constrain shallow structure such as the seafloor sediments. Inversion tests demonstrated that including *a priori* a realistic distribution of conductive ocean sediments was essential; anomalous phases of the nominal TE mode (coast-parallel electric field) impedances, both for onshore and offshore sites near the coast could not be fit without imposing this structure. Note that including a sediment layer greatly reduces the resistivity contrast at the seafloor, likely an important factor in improving performance of the inversion. Even with the sediment layer imposed fitting the offshore TE mode data was a challenge, which we found could be mitigated with a two-

stage inversion strategy: we first run the inversion with large error floors on the nominal TM mode (10% of the off-diagonal impedance), forcing the inversion to concentrate on fitting TE mode data, for which we used a smaller (5%) error floor. In the second stage the inversion was restarted, using 5% error floors for both modes. The final normalized root-mean-square (nRMS) misfit with 5% error floors was 2.74, with the largest misfits for TE mode data localized on the seafloor and near the coast (see Fig.

Responses for the full dataset (observed and computed) are shown as maps of apparent resistivity and phase in the SM in Figs.

5 Data availability

The data that support the findings of this study are publicly available online at http://ds.iris.edu/ds/products/emtf/.

6 Code availability

ModEM is freely available online at https://sites.google.com/site/modularem/ to the academic community.

References

1. Wang, K. & Tréhu, A. M. Invited review paper: Some outstanding issues in the study of great megathrust earthquakes—The Cascadia example. *Journal of Geodynamics* **98,** 1–18 (2016).
2. Wells, R. *et al.* Geologic history of Siletzia, a large igneous province in the Oregon and Washington Coast Range: Correlation to the geomagnetic polarity time scale and implications for a long-lived Yellowstone hotspot. *Geosphere* **10,** 692–719 (2014).
3. Irwin, W. P. *Geologic Map of the Klamath Mountains, California and Oregon* tech. rep. (US Geological Survey, 1994).
4. Greene, A. R. *et al.* The architecture of oceanic plateaus revealed by the volcanic stratigraphy of the accreted Wrangellia oceanic plateau. *Geosphere* **6,** 47–73 (2010).
5. Trehu, A. *et al.* Crustal architecture of the Cascadia forearc. *Science* **266,** 237–243 (1994).
6. Brandon, M. T. & Calderwood, A. R. High-pressure metamorphism and uplift of the Olympic subduction complex. *Geology* **18,** 1252–1255 (1990).
7. Gomberg, J., 2007, C. & Group, B. W. Slow-slip phenomena in Cascadia from 2007 and beyond: A review. *Bulletin* **122,** 963–978 (2010).
8. Rubinstein, J. L., La Rocca, M., Vidale, J. E., Creager, K. C. & Wech, A. G. Tidal modulation of nonvolcanic tremor. *Science* **319,** 186–189 (2008).
9. Rubinstein, J. L. *et al.* Seismic wave triggering of nonvolcanic tremor, episodic tremor and slip, and earthquakes on Vancouver Island. *Journal of Geophysical Research: Solid Earth* **114** (2009).
10. Liu, Y. & Rice, J. R. Spontaneous and triggered aseismic deformation transients in a subduction fault model. *Journal of Geophysical Research: Solid Earth* **112** (2007).
11. Peacock, S. M. Thermal and metamorphic environment of subduction zone episodic tremor and slip. *Journal of Geophysical Research: Solid Earth* **114** (2009).
12. Audet, P., Bostock, M. G., Christensen, N. I. & Peacock, S. M. Seismic evidence for overpressured subducted oceanic crust and megathrust fault sealing. *Nature* **457,** 76–78 (2009).
13. Audet, P., Bostock, M. G., Boyarko, D. C., Brudzinski, M. R. & Allen, R. M. Slab morphology in the Cascadia fore arc and its relation to episodic tremor and slip. *Journal of Geophysical Research: Solid Earth* **115** (2010).
14. Hansen, R. T., Bostock, M. G. & Christensen, N. I. Nature of the low velocity zone in Cascadia from receiver function waveform inversion. *Earth and Planetary Science Letters* **337,** 25–38 (2012).
15. Brudzinski, M. R. & Allen, R. M. Segmentation in episodic tremor and slip all along Cascadia. *Geology* **35,** 907–910 (2007).
16. Bostock, M. G., Christensen, N. I. & Peacock, S. M. Seismicity in Cascadia. *Lithos* **332,** 55–66 (2019).
17. Schmalzle, G. M., McCaffrey, R. & Creager, K. C. Central Cascadia subduction zone creep. *Geochemistry, Geophysics, Geosystems* **15,** 1515–1532 (2014).

18. Wells, R. E., Blakely, R. J., Wech, A. G., McCrory, P. A. & Michael, A. Cascadia subduction tremor muted by crustal faults. *Geology* **45,** 515–518 (2017).

19. Horning, G. *et al.* A 2-D tomographic model of the Juan de Fuca plate from accretion at axial seamount to subduction at the Cascadia margin from an active source ocean bottom seismometer survey. *Journal of Geophysical Research: Solid Earth* **121,** 5859–5879 (2016).

20. Canales, J. P., Carbotte, S. M., Nedimović, M. & Carton, H. Dry Juan de Fuca slab revealed by quantification of water entering Cascadia subduction zone. *Nature Geoscience* **10,** 864–870 (2017).

21. Han, S. *et al.* Seismic reflection imaging of the Juan de Fuca plate from ridge to trench: New constraints on the distribution of faulting and evolution of the crust prior to subduction. *Journal of Geophysical Research: Solid Earth* **121,** 1849–1872 (2016).

22. Han, S., Bangs, N. L., Carbotte, S. M., Saffer, D. M. & Gibson, J. C. Links between sediment consolidation and Cascadia megathrust slip behaviour. *Nature Geoscience* **10,** 954–959 (2017).

23. Han, S., Carbotte, S. M., Canales, J. P., Nedimović, M. R. & Carton, H. Along-Trench Structural Variations of the Subducting Juan de Fuca Plate From Multichannel Seismic Reflection Imaging. *Journal of Geophysical Research: Solid Earth* **123,** 3122–3146 (2018).

24. Abers, G. A. *et al.* Imaging the source region of Cascadia tremor and intermediate-depth earthquakes. *Geology* **37,** 1119–1122 (2009).

25. Calvert, A. J., Preston, L. A. & Farahbod, A. M. Sedimentary underplating at the Cascadia mantle-wedge corner revealed by seismic imaging. *Nature Geoscience* **4,** 545–548 (2011).

26. Delph, J. R., Levander, A. & Niu, F. Fluid controls on the heterogeneous seismic characteristics of the Cascadia margin. *Geophysical Research Letters* **45,** 11–021 (2018).

27. Hyndman, R. D. & Peacock, S. M. Serpentinization of the forearc mantle. *Earth and Planetary Science Letters* **212,** 417–432 (2003).

28. Saffer, D. M. & Tobin, H. J. Hydrogeology and mechanics of subduction zone forearcs: Fluid flow and pore pressure. *Annual Review of Earth and Planetary Sciences* **39,** 157–186 (2011).

29. Peacock, S. M., Christensen, N. I., Bostock, M. G. & Audet, P. High pore pressures and porosity at 35 km depth in the Cascadia subduction zone. *Geology* **39,** 471–474 (2011).

30. Audet, P. & Kim, Y. Teleseismic constraints on the geological environment of deep episodic slow earthquakes in subduction zone forearcs: A review. *Tectonophysics* **670,** 1–15 (2016).

31. Wannamaker, P. E. *et al.* Resistivity cross section through the Juan de Fuca subduction system and its tectonic implications. *Journal of Geophysical Research: Solid Earth* **94,** 14127–14144 (1989).

32. Wannamaker, P. E. *et al.* Segmentation of plate coupling, fate of subduction fluids, and modes of arc magmatism in Cascadia, inferred from magnetotelluric resistivity. *Geochemistry, Geophysics, Geosystems* **15,** 4230–4253 (2014).

33. Soyer, W. & Unsworth, M. Deep electrical structure of the northern Cascadia (British Columbia, Canada) subduction zone: Implications for the distribution of fluids. *Geology* **34,** 53–56 (2006).

34. Evans, R. L., Wannamaker, P. E., McGary, R. S. & Elsenbeck, J. Electrical structure of the central Cascadia subduction zone: The EMSLAB Lincoln Line revisited. *Earth and Planetary Science Letters* **402,** 265–274 (2014).

35. McGary, R. S., Evans, R. L., Wannamaker, P. E., Elsenbeck, J. & Rondenay, S. Pathway from subducting slab to surface for melt and fluids beneath Mount Rainier. *Nature* **511,** 338–340 (2014).

36. Schultz, A. EMScope: a continental scale magnetotelluric observatory and data discovery resource. *Data Science Journal* **8,** IGY6–IGY20 (2010).

37. Wells, R. E., Weaver, C. S. & Blakely, R. J. Fore-arc migration in Cascadia and its neotectonic significance. *Geology* **26,** 759–762 (1998).

38. Tabor, R. W. & Cady, W. M. *Geologic map of the Olympic Peninsula, Washington* tech. rep. (1978).

39. Duncan, R. A. A captured island chain in the Coast Range of Oregon and Washington. *Journal of Geophysical Research: Solid Earth* **87,** 10827–10837 (1982).

40. Wells, R., Engebretson, D., Snavely Jr, P. & Coe, R. Cenozoic plate motions and the volcano-tectonic evolution of western Oregon and Washington. *Tectonics* **3,** 275–294 (1984).

41. Bedrosian, P. A., Peacock, J. R., Bowles-Martinez, E., Schultz, A. & Hill, G. J. Crustal inheritance and a top-down control on arc magmatism at Mount St Helens. *Nature Geoscience* **11,** 865–870 (2018).

42. Peacock, S. M. Numerical simulation of metamorphic pressure-temperature-time paths and fluid production in subducting slabs. *Tectonics* **9,** 1197–1211 (1990).

43. Hacker, B. R. H2O subduction beyond arcs. *Geochemistry, Geophysics, Geosystems* **9** (2008).

44. Peacock, S. M., Wang, K. & McMahon, A. M. Thermal structure and metamorphism of subducting oceanic crust: Insight into Cascadia intraslab earthquakes. *The Cascadia Subduction Zone and Related Subduction Systems: Seismic Structure, Intraslab Earthquakes and Processes, and Earthquake Harzards* **2,** 123–126 (2002).

45. Fagereng, Å. & Diener, J. F. Non-volcanic tremor and discontinuous slab dehydration. *Geophysical research letters* **38** (2011).

46. Brandon, M. T., Roden-Tice, M. K. & Garver, J. I. Late Cenozoic exhumation of the Cascadia accretionary wedge in the Olympic Mountains, northwest Washington State. *Geological Society of America Bulletin* **110,** 985–1009 (1998).

47. Brandon, M. The Cascadia subduction wedge: the role of accretion, uplift, and erosion. *Earth structure: an introduction to structural geology and tectonics,* 566–574 (2004).

48. McNeill, L. C., Goldfinger, C., Kulm, L. D. & Yeats, R. S. Tectonics of the Neogene Cascadia forearc basin: Investigations of a deformed late Miocene unconformity. *Geological Society of America Bulletin* **112,** 1209–1224 (2000).

49. Moore, J. C. & Vrolijk, P. Fluids in accretionary prisms. *Reviews of Geophysics* **30,** 113–135 (1992).

50. Hyndman, R. D., McCrory, P. A., Wech, A., Kao, H. & Ague, J. Cascadia subducting plate fluids channelled to fore-arc mantle corner: ETS and silica deposition. *Journal of Geophysical Research: Solid Earth* **120,** 4344–4358 (2015).

51. Audet, P. & Schaeffer, A. J. Fluid pressure and shear zone development over the locked to slow slip region in Cascadia. *Science advances* **4,** eaar2982 (2018).

52. Bostock, M. The Moho in subduction zones. *Tectonophysics* **609,** 547–557 (2013).

53. Nedimović, M. R., Hyndman, R. D., Ramachandran, K. & Spence, G. D. Reflection signature of seismic and aseismic slip on the northern Cascadia subduction interface. *Nature* **424,** 416–420 (2003).

54. Calvert, A. J., Bostock, M. G., Savard, G. & Unsworth, M. J. Cascadia low frequency earthquakes at the base of an overpressured subduction shear zone. *Nature communications* **11,** 1–10 (2020).

55. Clowes, R. *et al.* LITHOPROBEÑsouthern Vancouver Island: Cenozoic subduction complex imaged by deep seismic reflections. *Canadian Journal of Earth Sciences* **24,** 31–51 (1987).

56. Kurtz, R., DeLaurier, J. & Gupta, J. A magnetotelluric sounding across Vancouver Island detects the subducting Juan de Fuca plate. *Nature* **321,** 596–599 (1986).

57. Bürgmann, R. The geophysics, geology and mechanics of slow fault slip. *Earth and Planetary Science Letters* **495,** 112–134 (2018).

58. Audet, P. & Bürgmann, R. Possible control of subduction zone slow-earthquake periodicity by silica enrichment. *Nature* **510,** 389–392 (2014).

59. Fagereng, Å., Diener, J. F., Meneghini, F., Harris, C. & Kvadsheim, A. Quartz vein formation by local dehydration embrittlement along the deep, tremorgenic subduction thrust interface. *Geology* **46,** 67–70 (2018).

60. Luo, Y. & Liu, Z. Rate-and-state model casts new insight into episodic tremor and slow-slip variability in Cascadia. *Geophysical Research Letters* **46,** 6352–6362 (2019).

61. Liu, L. & Hasterok, D. High-resolution lithosphere viscosity and dynamics revealed by magnetotelluric imaging. *Science* **353,** 1515–1519 (2016).

62. McCrory, P. A., Blair, J. L., Waldhauser, F. & Oppenheimer, D. H. Juan de Fuca slab geometry and its relation to Wadati-Benioff zone seismicity. *Journal of Geophysical Research: Solid Earth* **117** (2012).

63. Bedrosian, P. A. & Box, S. Subsurface geometry of the Siletz-Klamath suture in southwest Oregon from magnetotelluric imaging. *Geol. Soc. America annual mtg* (2007).

64. Aprea, C., Unsworth, M. & Booker, J. Resistivity structure of the Olympic mountains and Puget Lowlands. *Geophysical research letters* **25,** 109–112 (1998).

65. Egbert, G. D. & Booker, J. R. Robust estimation of geomagnetic transfer functions. *Geophysical Journal International* **87,** 173–194 (1986).

66. Egbert, G. D. Robust multiple-station magnetotelluric data processing. *Geophysical Journal International* **130,** 475–496. ISSN: 0956-540X (Aug. 1997).

67. Kelbert, A., Meqbel, N., Egbert, G. D. & Tandon, K. ModEM: A modular system for inversion of electromagnetic geophysical data. *Computers & Geosciences* **66,** 40–53 (2014).

68. Booker, J. R., Favetto, A. & Pomposiello, M. C. Low electrical resistivity associated with plunging of the Nazca flat slab beneath Argentina. *Nature* **429,** 399–403. ISSN: 0028-0836. (2015) (May 2004).

69. Straume, E. O. *et al.* GlobSed: Updated Total Sediment Thickness in the World's Oceans. *Geochemistry, Geophysics, Geosystems* **20.** 5, 1756–1772. ISSN: 1525-2027 (2019).

70. Cox, C., Constable, S., Chave, A. & Webb, S. Controlled-source electromagnetic sounding of the oceanic lithosphere. *Nature* **320,** 52–54 (1986).

71. Worzewski, T., Jegen, M., Kopp, H., Brasse, H. & Castillo, W. T. Magnetotelluric image of the fluid cycle in the Costa Rican subduction zone. *Nature Geoscience* **4,** 108–111 (2011).

72. Schmandt, B. & Humphreys, E. Complex subduction and small-scale convection revealed by body-wave tomography of the western United States upper mantle. *Earth and Planetary Science Letters* **297,** 435–445 (Sept. 2010).

73. Naif, S., Key, K., Constable, S. & Evans, R. Melt-rich channel observed at the lithosphere–asthenosphere boundary. *Nature* **495,** 356–359 (2013).

Acknowledgements: This work was supported by NSF grants EAR1053632 and EAR1460437 (G.E. and A.S.), EAR1053207 and EAR1459067 (K.K.), EAR1053202 and EAR140552 (D.L.), NSFC grant 41774079, and National Key R&D Program of China 2018YFC0603604 (B.Y.).

Author Contributions:

D.L., K.K., A.S. and P.B. collected the new MT data. A.K. processed the new land data and K.K. processed the marine data. B.Y. and B.P. ran 3D inversions. G.E., B.Y. and P.B. developed the interpretation, and wrote the manuscript, with input from all other authors.

Competing Interests:

The authors declare no competing interests.

Supplementary Files

This is a list of supplementary files associated with this preprint. Click to download.

- MOCHASM.pdf